Supplemental Information

Synthetic Incoherent Feedforward Circuits Show Adaptation to the Amount of their Genetic Template.

Leonidas Bleris, Zhen Xie, David Glass, Asa Adadey, Eduardo Sontag, Yaakov Benenson

Supplemental Figures

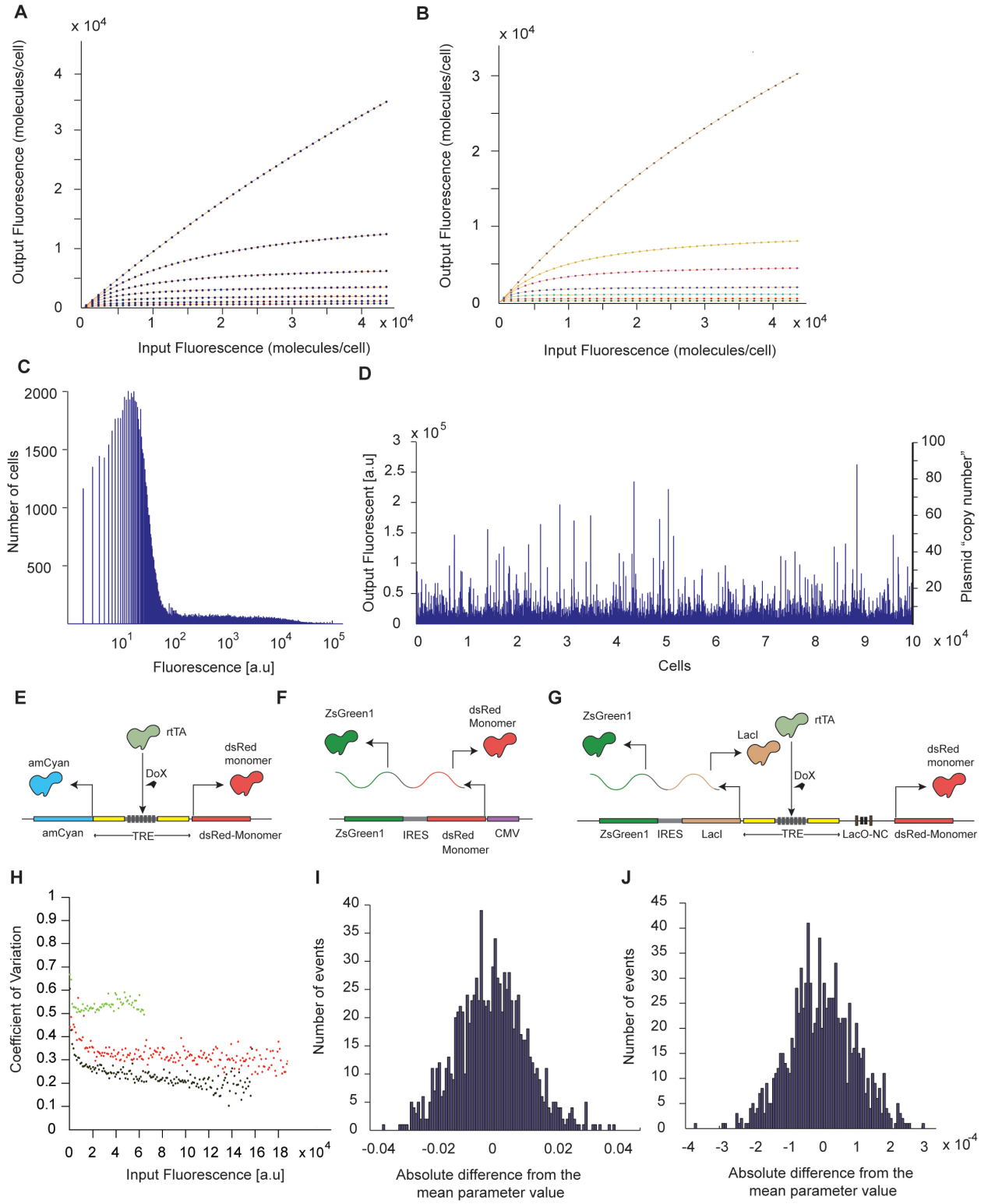

Supplementary Figure 1. Simulation details. (**A**) Parametric simulations of the transcriptional I1-

FFL input-output behavior (dots) for a range of binding constants (Figure 2B) and the fitting to the rational function $\sigma(x)=c(x+a)/(x+b)$ (orange curves). (**B**) Parametric simulations of the post-transcriptional I1-FFL_I input-output behavior (dots) for a range of RNAi degradation rates (Figure 2F) and the fitting to the rational function $\sigma(x)=c(x+a)/(x+b)$ (orange curves). (**C**) Histogram of ZsGreen fluorescent protein levels in transiently-transfected cells measured using flow cytometry. In this experiment, 400 ng of plasmid carrying constitutively-expressed, CMV-driven LacI-IRES-zsGreen1 construct was transfected into HEK293 TET-On cells and measured after 48 hours. (**D**) "Time series" of the fluorescence level in single cells, picked from the distrbution in panel C and used for noisy simulations. The first Y axis shows fluorescence in instrument units, the second axis shows this intensity converted to a "copy-number" using an arbitrary scaling factor. (**E-H**) Constructs used to characterize the intrinsic noise of the pTRE promoter and the IRES element. All experiments were performed in the presence of 1000 ng/ml Dox. (**E**) A construct pTRE-Tight-BI-amCyan-DsRed with a pTRE bidirectional promoter driving the expression of amCyan and DsRed. (**F**) A construct DsRed-pIRES2-zsGreen1 constituvely driving the expression of a single IRES-connected ZsGreen1/DsRed-encoding transcript. (**G**) Transcriptional I1-FFL construct with a fully mutated LacO sequence, pTRE-Tight-BI-LacI-IRES-ZsGreen1-$LacO_{NegCtrl}$-DsRed. (**H**) Measured coefficient of variation of one fluorescent output level for a given level of another protein designated as input. pTRE-Tight-BI-LacI-IRES-ZsGreen1-$LacO_{NegCtrl}$-DsRed is shown in green (input: ZsGreen, output: DsRed), DsRed-pIRES2-zsGreen1 in shown in red (input: ZsGreen, output: DsRed), and pTRE-Tight-BI-amCyan-DsRed is shown in black (input: DsRed, output: AmCyan). (**I, J**) Normal distributions used for incorporating noise in "noisy" simulations. (**I**) Normal distribution characterizing pTRE promoter, rescaled to have the mean value of zero and standard deviation equaling to 25% of

0.0467 sec^{-1}, the rate of expression from pTRE proimoter used in simulations. (**J**) A normal distribution characterizing the IRES element, rescaled to have the mean value of zero mean and standard deviation equaling to 30% of 0.00033 sec^{-1}, the basic translation rate used in simulations.

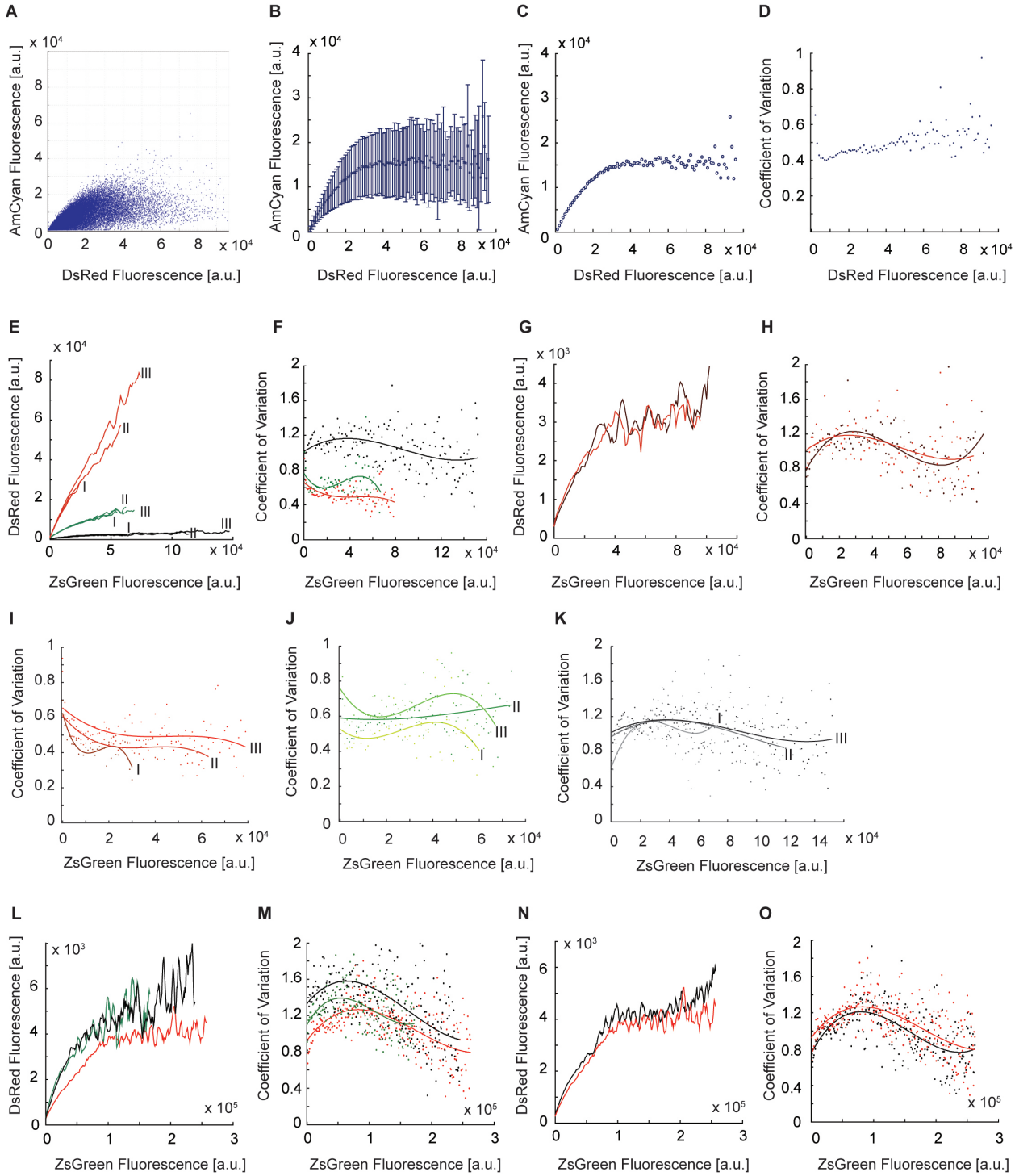

Supplementary Figure 2. Experimental implemenation of the circuits. (**A**) An example of raw flow cytometry data measured with post-transcriptional I1-FFL circuit. (**B-D**) An illustration of

the binning processing using data from panel A. (**B**) The mean value and the standard deviation of the output values in each bin of 1000 fluorescence units. (**C**) The plot of mean values for each bin. (**D**) The plot of coefficient of variation values for each bin. (**E-H**) Titration of plasmid and Dox concentration for the transcriptional I1-FFL. (**E**) I, II and III indicate 200, 400 and 800 ng of the circuit-encoding plasmid, respectively. Red, green and black color indicate LacO mutant 4, LacO mutant 1 and wild-type LacO, respectively. These experiments were performed using Lipofectamine PLUS transfection reagents with 1000 ng/ml Dox. (**F**) Coefficients of variation measured with different LacO variants with red, green and black color corresponding to 800 ng of LacO mutant 4, LacO mutant 1 and wild-type LacO, respectively. (**G**) Input-output response with different Dox concentrations. 1000 ng of the wild type LacO tI1-FFL circuit plasmid were transfected in the presence of 1000 ng/mL (red) or 4000 ng/mL (black) Dox. (**H**) Coefficients of variation measured for the experiments in panel G, using the same color coding. (**I-K**). Coefficients of variation measured in all the experiments shown in panel E. Latin numerals and color-coding are the same. (**L-O**) Effects of different transfection reagents and wait times prior to measurements on the transcriptional I1-FFL. (**L**) 1000 ng of the wild type I1-FFL using Lipofectamine 2000 (black), 500 ng of the wild type I1-FFL using Lipofectamine-PLUS (green), and 500 ng of the wild type I1-FFL using LipoLTX (red). All the experiments are performed in the presence of 1000 ng/ml Dox. (**M**) Coefficient of variation for the experiments detailed in panel L using the same color-coding. (**N**) 500 ng of the wild type I1-FFL transfected using LipoLTX measured 48h post-tranfection (red) and 72h post-transfection (black). (**O**) Coefficient of variation for the experiments detailed in panel C, same color-coding.

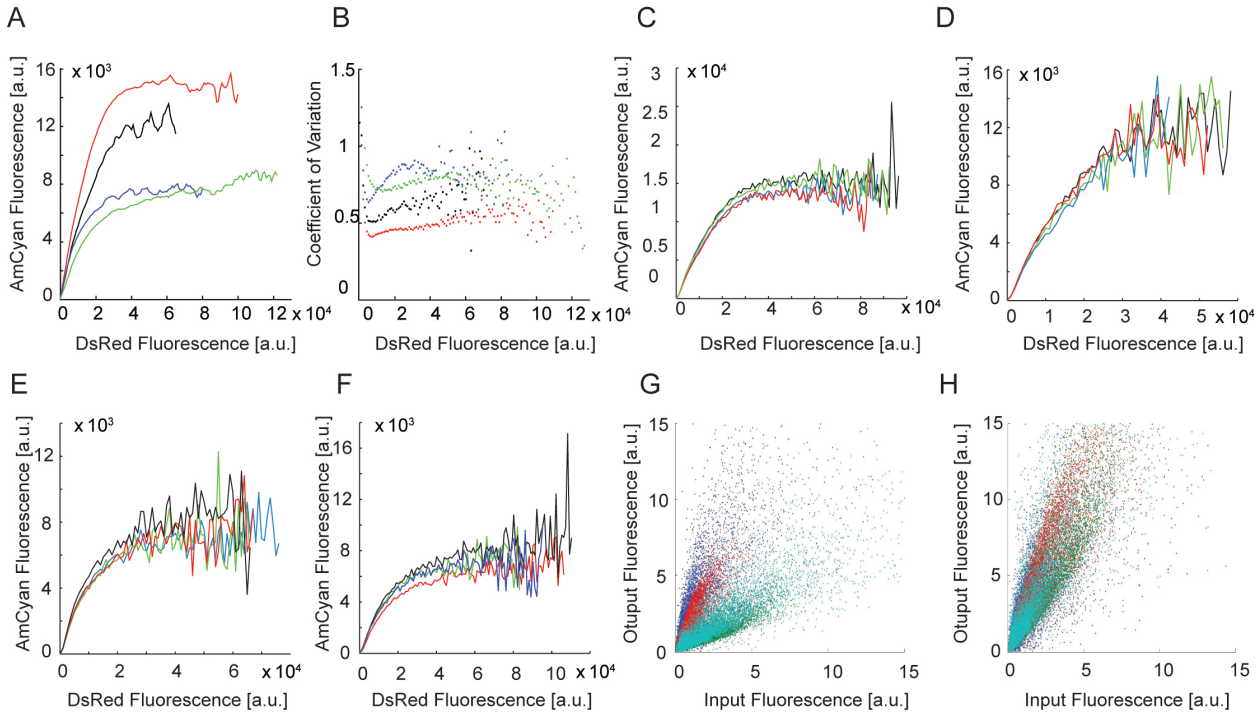

Supplementary Figure 3. Calibration of experimental conditions for the post-transcriptional I1-FFL, version I. (**A, B**) Titration of concentrations and comparison of transfection reagents. (**A**) 250 ng of the ptI1-FFL-ver1 using Lipofectamine PLUS (blue), 500ng of the ptI1-FFL-ver1 using Lipofectamine PLUS (black), 500 ng of the ptI1-FFL-ver1 using Lipofectamine 2000 (green), and 500 ng of the ptI1-FFL-ver1 using LipoLTX (red). All the experiments are performed in the presence of 1000 ng/ml Dox. (**B**) Coefficient of variation measured in the experiments detailed in panel a using the same color-coding. (**C-F**) Reproducibility of the input-output behavior observed with different combinations of plasmid amounts and transfection reagents used in panel A. (**C**) Four repeats transfecting 500 ng of the ptI1-FFL-ver1 using LipoLTX (same conditions as the red curve in panel A). (**D**) Four repeats transfecting 500 ng of the ptI1-FFL-ver1 using Lipofectamine PLUS (same conditions as the black curve in panel A). (**E**) Four repeats transfecting 250 ng of the ptI1-FFL-ver1 using Lipofectamine PLUS (same

conditions as the blue curve in panel A). (**F**) Four repeats transfecting 500 ng of the ptI1-FFL-ver1 using Lipofectamine 2000 (same conditions as the green curve in panel A). (**G, H**) Illustration of the normalization procedure used to compare different circuits with different input and output fluorophores. (**G**) Raw scatter plots of the negative control of the four different constructs (blue: tI1-FFL, green: I1-FFL-ver1, red: I1-FFL-ver2, cyan: tAM). (**H**) Normalized scatter plots. 20,000 cells are shown for illustration.

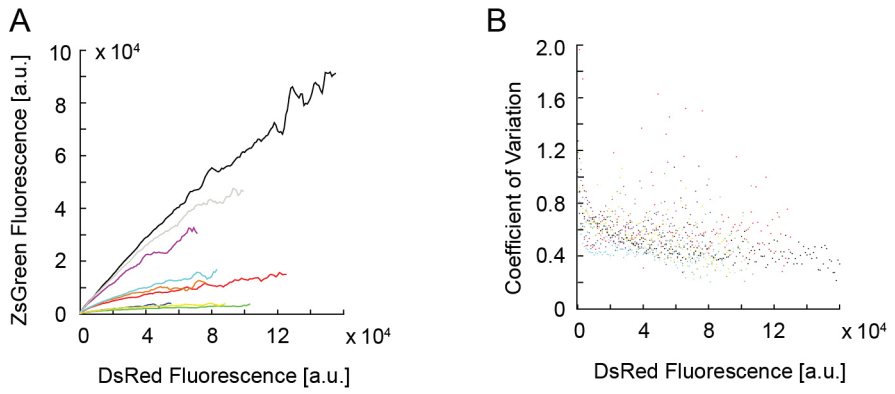

Supplementary Figure 4. Effect of transfection reagents for the transcriptional negative autoregulator. All experiments are performed using 500 ng of the plasmid in the presence of 1000 ng/ml Dox. (**A**) LipoLTX reagent: 2xLaO trAM (green), 1xLaO trAM (red), and 1xLacO trAM with 1M IPTG (black). Lipofectamine Plus: 2xLaO trAM (blue), 1xLaO trAM (orange), and 1xLacO trAM with 1M IPTG (purple). Lipofectamine 2000: 2xLaO trAM (yellow), 1xLaO trAM (cyan), and 1xLacO trAM with 1M IPTG (gray). (**B**) Coefficient of variation for all the experiments in panel A, using the same color-coding.

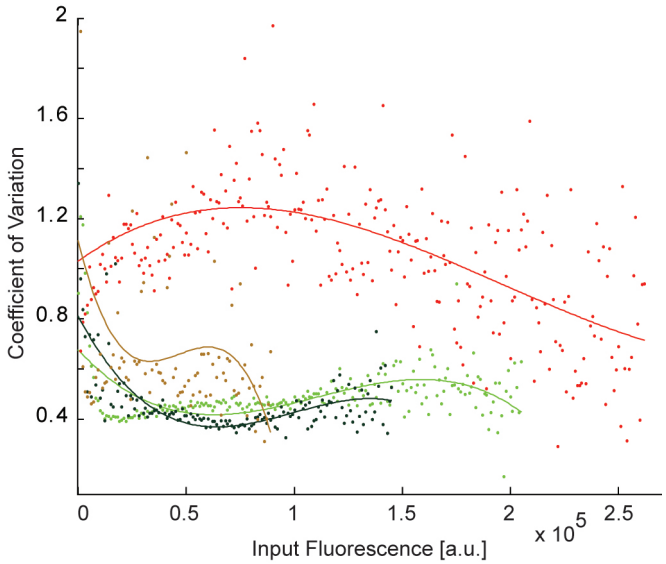

Supplementary Figure 5. Coefficient of variation for the motifs. Coefficient of variation in individual bins for each of the circuits; red: transcriptional incoherent feedforward loop; brown: transcriptional autoregulation; green: post-transcriptional incoherent feedforward motif version I; black: post-transcriptional incoherent feedforward motif version II.

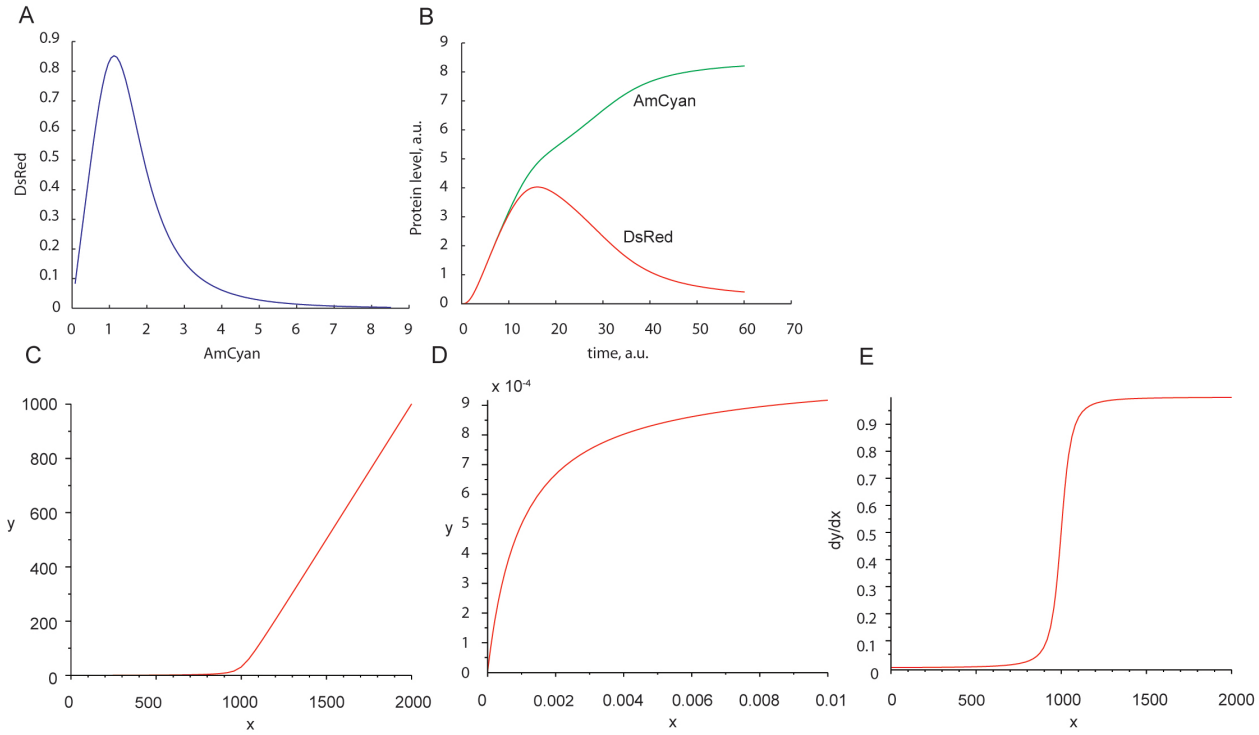

Supplementary Figure 6. Analytical simulations of the circuits. (**A**) Steady state levels of output (DsRed) vs input (AmCyan) in a special case of biphasic behavior. (**B**) Dynamic development of the input and output levels in biphasic case. (**C**) Plot of output (y) vs input (x) for post-transcriptional circuit showing almost constant behavior for x < 500 and linear behavior (y = x + constant) for large x, as predicted from approximate analysis. (**D**) Zooming in the plot in panel C to show initial saturation behavior at y = 0:001. (**E**) Plot of derivative dy/dx, showing both an almost zero initial slope (adaptation) and an eventual nonzero constant slope (linear regime).

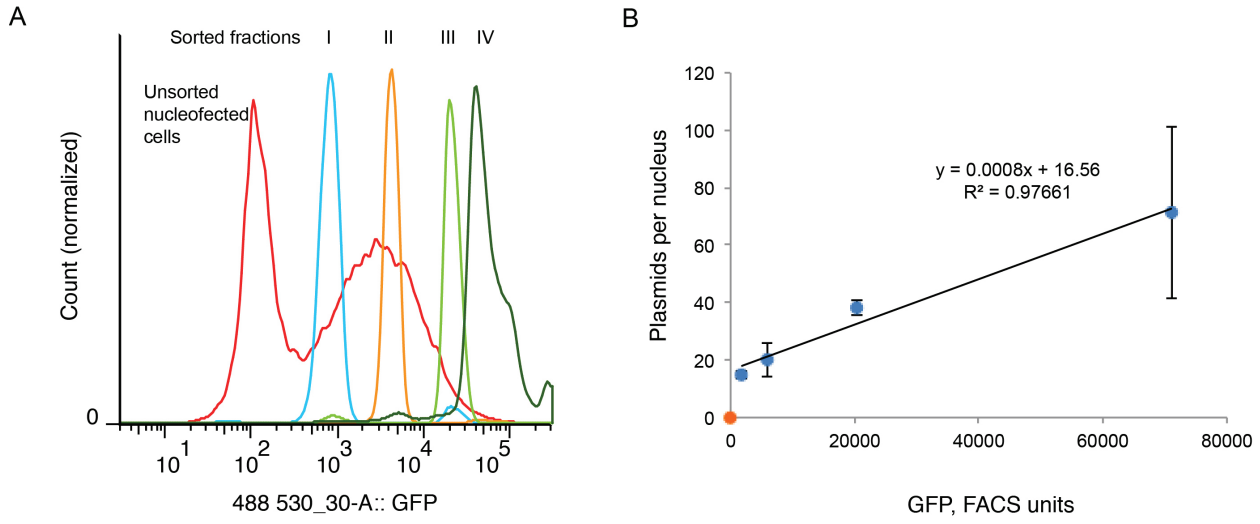

Supplementary Figure 7. Quantification of the relation between fluorescence and plasmid copy number. (**A**) Flow cytometry analysis of four FACS-sorted cell fractions overlaid on the flow cytometry distribution of the original unsorted population. Note that each fraction is normalized to the highest value in its own group. (B) Quantitative results of qPCR measurements, normalized to an internal control gene ACTB and based on the assumption that most 293 cells are triploid (based on ATCC record).

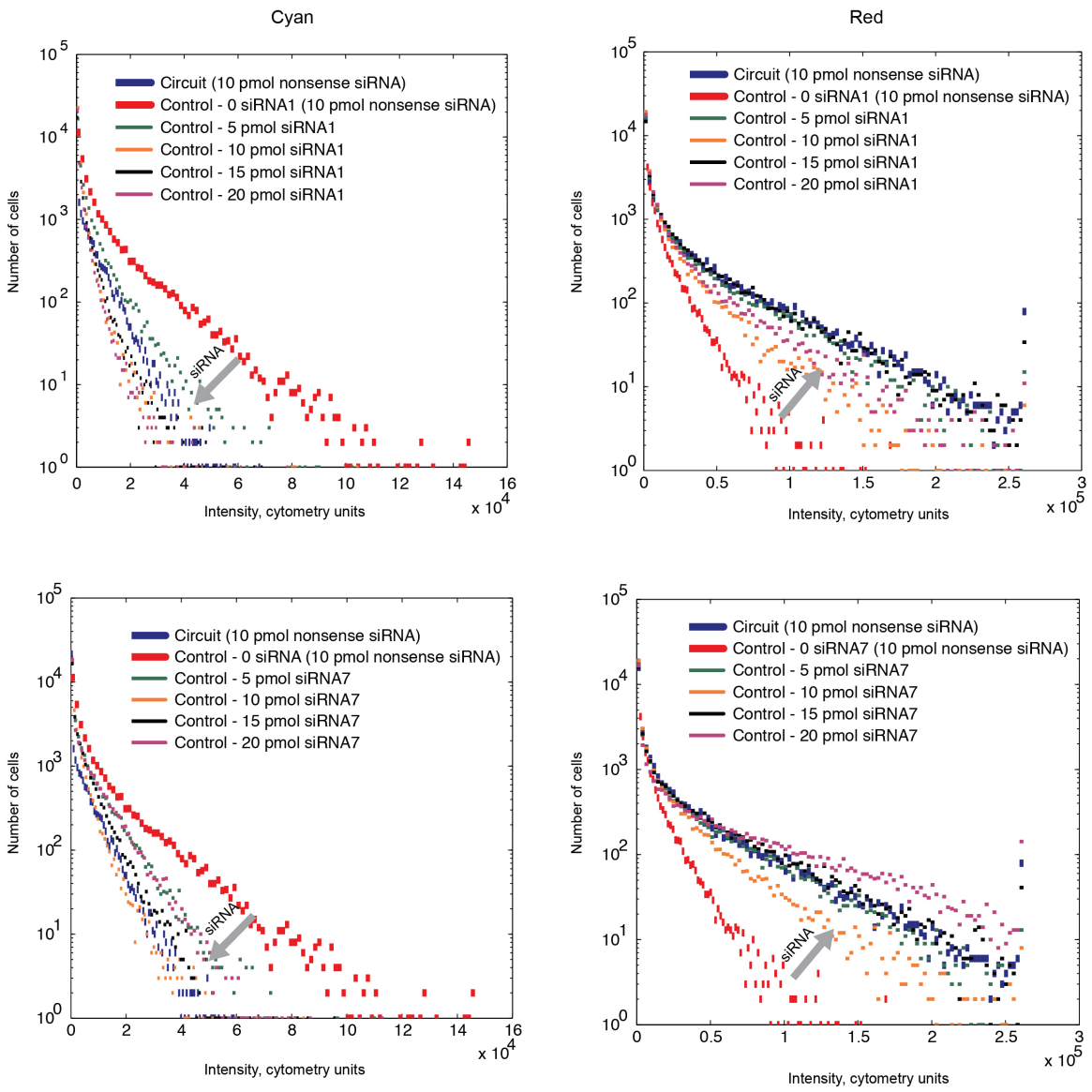

Supplementary Fig. 8. Effect of RNAi-induced knockdown of the output on the distribution of the input in ptI1-FFL$_I$. Histograms of AmCyan and DsRed obtained in flow cytometry experiments are shown as indicated. The top row shows data obtained with anti-AmCyan siRNA-1 and the bottom row shows data measured with anti-AmCyan siRNA-7.

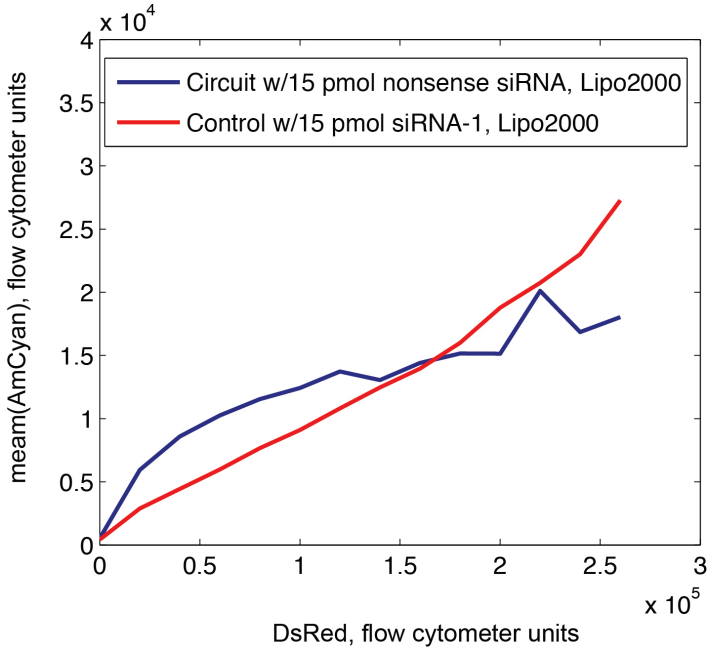

Supplementary Figure 9. siRNA-induced knock-down of AmCyan in a control circuit does not lead to adaptive input-output relationship. A representative comparison is shown, in which the distributions of both AmCyan and DsRed are similar between the siRNA-targeted control and the circuit. Despite similarity of the cumulative distributions, the siRNA-targeted control does not exhibit adaptive behavior.

Supplemental Tables

Supplementary Table 1. Estimated parameter values of the fit of the simulated tI1-FFL and pI1-FFL_I to the rational function **y=σ(x)=c(x+a)/(x+b)**.

Motif	LacI K_{on}	a	b (EC_{50})	c	R^2
tI1-FFL	3.3300e-7	-0.058667	1.7087e5	1.7092e5	1.00
tI1-FFL	3.3300e-6	1.6532	17583	17401	1.00
tI1-FFL	8.3250e-6	3.2408	7720.6	7246.6	1.00
tI1-FFL	1.6650e-5	3.8466	4504.6	3813.7	1.00
tI1-FFL	3.3300e-5	4.6685	3013.5	2062.6	1.00
tI1-FFL	6.6600e-5	7.4365	2601.9	1171.1	0.99
tI1-FFL	1.3320e-4	19.799	3488.3	731.82	0.99
Motif	miRNA K_{on}	a	b (EC_{50})	c	R^2
pI1-FFL_I	1.84e-9	0.016157	98518	98614	1.00
pI1-FFL_I	1.84e-8	0.0014108	9849.4	9859.4	1.00
pI1-FFL_I	3.7e-8	-3.1354e-4	4924.7	4929.8	1.00
pI1-FFL_I	9.2e-8	1.5222e-4	1969.9	1971.8	1.00
pI1-FFL_I	1.84e-7	-2.364e-5	984.84	985.93	1.00
pI1-FFL_I	4.6e-7	3.5341e-5	393.99	394.37	1.00
pI1-FFL_I	1.84e-6	2.3436e-6	98.462	98.591	1.00

Supplementary Table 2. Estimated parameter values, their confidence intervals and the coefficient of determination of the fit to the rational function **y=σ(x)=c(x+a)/(x+b)** calculated for the input-output dependency of the different circuits.

Motif	Variant	a	Conf. Int.	b (EC_{50})	Conf. Int.	C	Conf. Int.	R^2
tI1-FFL	Wild Type	-988.27	2000.8	53959	8521.7	5475.9	188.2	0.93
tI1-FFL	Mutant 1	6699.5	2937	197930	37162	72973	6955	0.97
tI1-FFL	Mutant 2	10148	3376	276860	58344	168460	20428	0.97
tI1-FFL	Mutant 3	5887.2	2136	274860	38380	219650	17567	0.99
tI1-FFL	Mutant 4	3573.7	873	205640	29838	335980	33218	1.00
tI1-FFL	Neg. Con.	2042.6	732	145750	30550	388250	57629	1.00
$pI1\text{-}FFL_I$	1xF3	-3192.4	849	27955	3423	54677	1236.3	0.96
$pI1\text{-}FFL_I$	Neg. Con.	796.01	131.6	113030	4461.4	349250	9269.1	1.00
$pI1\text{-}FFL_{II}$	1xF3	-2939.6	1215	82128	11617	95712	5562	0.98
$pI1\text{-}FFL_{II}$	Neg. Con.	-1018.2	260.3	6.29e15	1.0179e24	1.18e16	1.9215e24	1.00
tAM	2xLacO	6209.9	2683	71764	26481	11685	2078	0.96
tAM	1xLacO	5511.9	1732	128100	31346	66880	9639	0.99
tAM	Neg. Con.	368.89	530	233110	48744	541510	89683	1.00

Supplementary Table 3. Estimated parameter values, their confidence intervals and the coefficient of determination of the fit to the function $\boldsymbol{\pi_1(x)} = -a+(a^2+bx)^{1/2}$ calculated for the input-output dependency of the different circuits.

Motif	Variant	a	Conf. Int.	b	Conf. Int.	c	Conf. Int.	R^2
tI1-FFL	Wild Type	818.1	599.82	2.62e6	1.29e7	0.3168	0.0551	0.87*
tI1-FFL	Mutant 1	950.64	1514.9	446.07	665.3	0.5786	0.0457	0.98*
tI1-FFL	Mutant 2	-227.64	25227	287.54	376.9	0.6283	0.0448	0.98*
tI1-FFL	Mutant 3	1869.1	2476.9	290.6	280.1	0.6432	0.0337	0.99*
tI1-FFL	Mutant 4	-927.7719	1500	76.0176	38	0.7353	0.0228	1.00*
tI1-FFL	Neg. Con.	-949.13	2010.4	80.524	50.7	0.7585	0.0304	1.00*
$pI1\text{-}FFL_I$	1xF3	-7911.5	7026.5	8.97e9	6.41e10	0.3126	0.0607	0.85*
$pI1\text{-}FFL_I$	Neg. Con.	-1299.4	1579.6	106.7	51.2625	0.7498	0.0226	1.00*
$pI1\text{-}FFL_{II}$	1xF3	-9740.4	4192.2	49555	130700	0.4930	0.0554	0.96*
$pI1\text{-}FFL_{II}$	Neg. Con.	805.429	359.99	0.7892	0.0751	1.08	0.0094	1.00*
tAM	2xLacO	451	381.7211	65.6953	138.4487	0.5664	0.0749	0.97*
tAM	1xLacO	945.6381	909.4237	80.4426	92.2213	0.6502	0.0460	0.99*
tAM	Neg. Con.	-967.2	1929.7	14.9831	8.4	0.8490	0.341	1.00*
*fitting algorithm reached maximum number of iterations								

Supplementary Table 4. Estimated parameter values, their confidence intervals and the coefficient of determination of the fit to the function $\boldsymbol{\pi_2(x)}$ =a+(bx)^c calculated for the input-output dependency of the different circuits.

Motif	Variant	a	Conf. Int.	b	Conf. Int.	R^2
tI1-FFL	Wild Type	323.05	117.92	82.52	6.8296	0.85
tI1-FFL	Mutant 1	5606.6	1294.7	9602.1	651.3431	0.98
tI1-FFL	Mutant 2	13052	2680.3	37254	2533	0.98
tI1-FFL	Mutant 3	27637	3654	72419	4215.3	0.99
tI1-FFL	Mutant 4	49847	5375	2.4166e5	14514	1.00
tI1-FFL	Neg. Con.	63773	9289	4.7344e5	41534	1.00
pI1-FFL$_I$	1xF3	-3903.5	1519.4	11815	1214.9	0.82
pI1-FFL$_I$	Neg. Con.	77424	4692	5.7462e5	22339	1.00
pI1-FFL$_{II}$	1xF3	14299	4239.3	39971	4629.8	0.96
pI1-FFL$_{II}$	Neg. Con.	5.5622e12	1.5904e13	2.0471e13	5.854e13	1.00
tAM	2xLacO	-120.51	148.91	546.15	39.59	0.97
tAM	1xLacO	4102.6	1047.5	12112	894.5	0.97
tAM	Neg. Con.	175470	27590	861240	108980	1.00

Supplementary Table 5. Estimated parameter values, their confidence intervals and the coefficient of determination of the fit to the linear function $\lambda(x)=a+bx$ calculated for the experimentally-measured input-output dependency of the different circuits.

Motif	Variant	a	Conf. Int.	b	Conf. Int.	R^2
tI1-FFL	Wild	0.01303	0.001	1746.2	148.5616	0.72

	Type					
tI1-FFL	Mutant 1	0.17378	0.0058	7005.6	642.8080	0.95
tI1-FFL	Mutant 2	0.33418	0.0097	12974	1103.4	0.96
tI1-FFL	Mutant 3	0.43472	0.0109	14459	1287.4	0.97
tI1-FFL	Mutant 4	1.0871	0.0250	12927	1357.9	0.99
tI1-FFL	Neg. Con.	1.8497	0.0513	12148	1753.3	0.99
pI1-FFL_I	1xF3	0.16801	0.0172	19924	1989	0.65
pI1-FFL_I	Neg. Con.	2.0203	0.0587	10864	1905.8	0.99
pI1-FFL_{II}	1xF3	0.40273	0.0218	9584.5	1768.5	0.91
pI1-FFL_{II}	Neg. Con.	1.8878	0.0144	-1923.5	499.2941	1.00
tAM	2xLacO	0.072899	0.0044	1682.4	176.5924	0.94
tAM	1xLacO	0.2947	0.011	5260.9	536.4035	0.97
tAM	Neg. Con.	1.8222	0.0361	5545.5	1297.1	1.00

Supplemental Experimental Procedures

1. Simulations

1.1. Deterministic simulations

Simbiology diagram used to simulate a transcriptional incoherent motif is shown below:

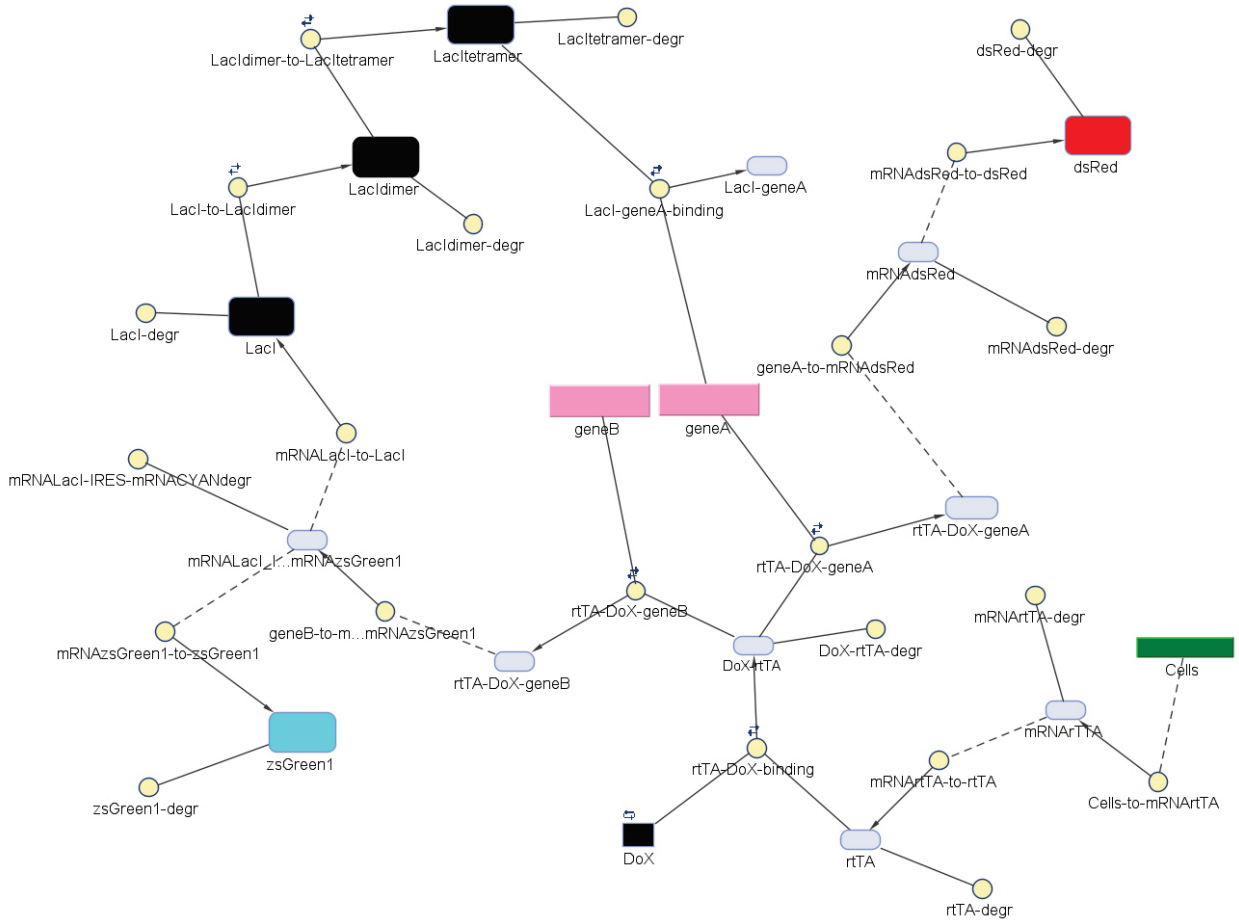

This diagram corresponds to the following reaction array:

[rtTA-DoX-geneA] -> mRNAdsRed + [rtTA-DoX-geneA]
mRNAdsRed -> dsRed + mRNAdsRed
mRNAdsRed -> null
dsRed -> null
geneA + LacItetramer <-> [LacI-geneA]

zsGreen1 -> null
mRNALacI_IRES_mRNAzsGreen1 -> zsGreen1 + mRNALacI_IRES_mRNAzsGreen1
[rtTA-DoX-geneB] -> [rtTA-DoX-geneB] + mRNALacI_IRES_mRNAzsGreen1
[DoX-rtTA] -> null
rtTA -> null
[DoX-rtTA] + geneB <-> [rtTA-DoX-geneB]
DoX + rtTA <-> [DoX-rtTA]
[DoX-rtTA] + geneA <-> [rtTA-DoX-geneA]
LacI -> null
LacItetramer -> null
mRNALacI_IRES_mRNAzsGreen1 -> LacI + mRNALacI_IRES_mRNAzsGreen1
2 LacI <-> LacIdimer
2 LacIdimer <-> LacItetramer
LacIdimer -> null
mRNALacI_IRES_mRNAzsGreen1 -> null
Cells -> Cells + mRNArTTA
mRNArTTA -> null
mRNArTTA -> mRNArTTA + rtTA

The parameters used in simulations are as follows:

	Value	Units	Reference
k-geneA-to-mRNAdsRed	0.0467	1/second	(Tigges et al, 2009)
k-mRNAdsRed-to-dsRed	0.00033333	1/second	(Tigges et al, 2009;Tigges et al, 2010)
k-mRNAdsRed-degr	0.00034	1/second	(Tigges et al, 2009)
k-dsRed-degr	0.000096667	1/second	(Tigges et al, 2009)
kON-LacI-geneA-binding	0.0000333	1/(molecule*second)	(Ozbudak et

			al, 2004)
kOFF-LacI-geneA-binding	0.001	1/second	(Ozbudak et al, 2004)
k-zsGreen1-degr	0.000096667	1/second	(Tigges et al, 2009)
k-mRNAzsGreen1-to-zsGreen1	0.00033333	1/second	(Tigges et al, 2009;Tigges et al, 2010)
k-geneB-to-mRNALacI_IRES_mRNACyan	0.0467	1/second	(Tigges et al, 2009)
k-DoX-rtTA-degr	0.000096667	1/second	(Tigges et al, 2009)
k-rtTA-degr	0.000096667	1/second	(Tigges et al, 2009)
kON-rtTA-DoX-geneB-binding	0.000000028	1/(molecule*second)	(Tigges et al, 2009)
kOFF-rtTA-DoX-geneB-binding	0.00001	1/second	(Tigges et al, 2009)
kON-rtTA-DoX-binding	0.00001	1/(molecule*second)	(To & Maheshri, 2010)
kOFF-rtTA-DoX-binding	0.00000002	1/second	(To & Maheshri, 2010)
kOFF-rtTA-DoX-geneA-binding	0.00001	1/second	(Tigges et al, 2009)
kON-rtTA-DoX-geneA-binding	0.000000028	1/(molecule*second)	(Tigges et al, 2009)
k-LacI-degr	0.000096667	1/second	(Tigges et al, 2009)
k-LacItetramer-degr	0.000096667	1/second	(Tigges et al,

			2009)
k-mRNALacI-to-LacI1	0.00033333	1/second	(Tigges et al, 2009;Tigges et al, 2010)
kON-LacI-to-LacIdimer	0.0004637	1/(molecule*second)	(Hsieh & Brenowitz, 1997)
kOFF-LacI-to-LacIdimer	0.00000001	1/second	(Hsieh & Brenowitz, 1997)
kON-LacIdimer-to-LacItetramer	0.000602	1/(molecule*second)	(Hsieh & Brenowitz, 1997)
kOFF-LacIdimer-to-LacItetramer	0.000001	1/second	(Hsieh & Brenowitz, 1997)
k-LacIdimer-degr	0.000096667	1/second	(Tigges et al, 2009)
k-mRNALacI-IRES-mRNAZsGreen1-degr	0.00034	1/second	(Tigges et al, 2009)
k-Cells-to-mRNArtTA	0.0467	1/second	(Tigges et al, 2009)
k-mRNrtTA-degr	0.00034	1/second	(Tigges et al, 2009)
k-mRNArtTA-to-rtTA	0.00033333	1/second	(Tigges et al, 2009;Tigges et al, 2010)

Simbiology diagram used to simulate a post-transcriptional incoherent motif is shown below:

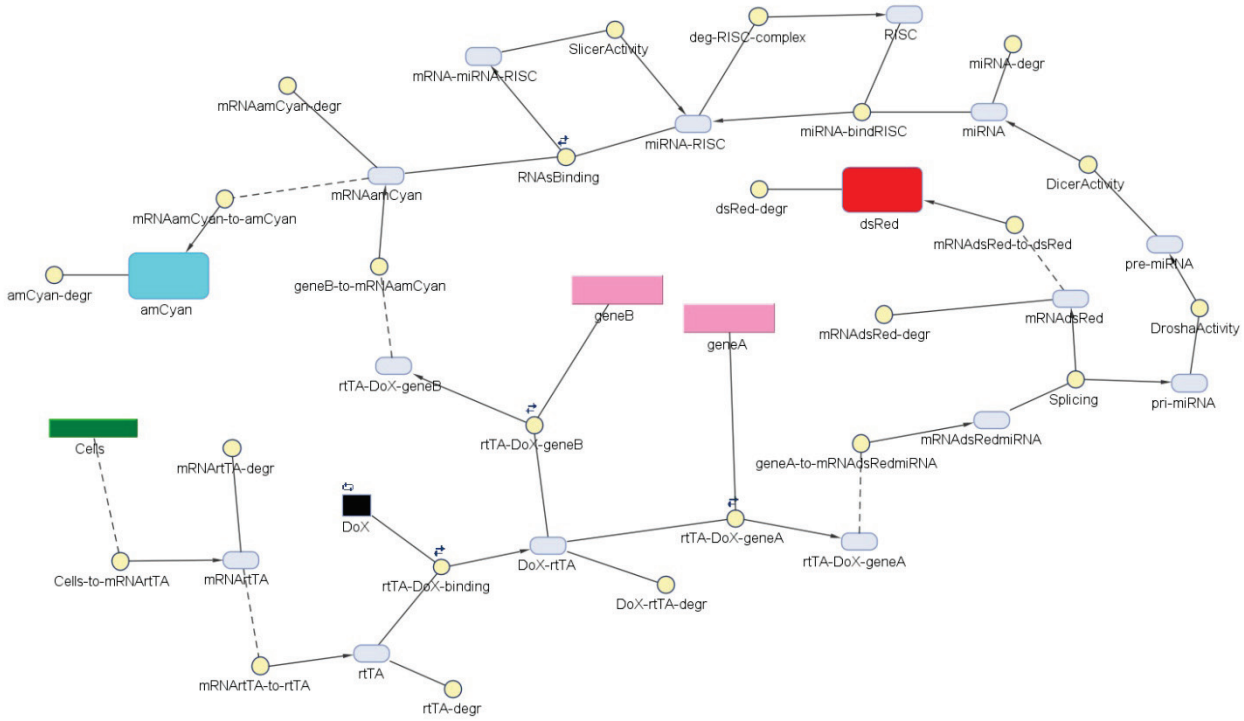

This diagram coresponds to the following reaction array:

[rtTA-DoX-geneA] -> mRNAdsRedmiRNA + [rtTA-DoX-geneA]
mRNAdsRed -> mRNAdsRed + dsRed
mRNAdsRedmiRNA -> [pri-miRNA] + mRNAdsRed
[pri-miRNA] -> [pre-miRNA]
[pre-miRNA] -> miRNA
miRNA_RISC + mRNAamCyan <-> mRNA_miRNA_RISC
mRNA_miRNA_RISC -> miRNA_RISC
dsRed -> null
mRNAdsRed -> null
miRNA -> null
miRNA_RISC -> RISC
miRNA + RISC -> miRNA_RISC
mRNArTTA -> mRNArTTA + rtTA
mRNArTTA -> null

Cells -> Cells + mRNArTTA
mRNAamCyan -> null
[DoX-rtTA] + geneA <-> [rtTA-DoX-geneA]
DoX + rtTA <-> [DoX-rtTA]
[DoX-rtTA] + geneB <-> [rtTA-DoX-geneB]
rtTA -> null
[DoX-rtTA] -> null
[rtTA-DoX-geneB] -> [rtTA-DoX-geneB] + mRNAamCyan
mRNAamCyan -> amCyan + mRNAamCyan
amCyan -> null

The parameters used in simulations are as follows:

	Value	Units	Reference
k_geneA-to-mRNAdsRedmiRNA	0.0467	1/second	(Tigges et al, 2009)
k_ mRNAdsRed-to-dsRed	0.000333	1/second	(Tigges et al, 2009;Tigges et al, 2010)
k_Splicing	0.002	1/second	Estimate
k_Drosha	0.01	1/second	Estimate
k_Dicer	0.001	1/second	(Tigges et al, 2010)
k_RISC_formation	0.00000184	1/(molecule*second)	(Tigges et al, 2010)
k_RISC_de-formation	0.01	1/second	(Tigges et al, 2010)
k_Slicer	0.007	1/second	(Tigges et al, 2010)
k_dsRed-degr	0.000096667	1/second	(Tigges et al, 2009)

k_mRNAdsRed-degr	0.000288	1/second	(Tigges et al, 2009)
k_miRNA-degr	0.000288	1/second	(Tigges et al, 2009)
k_RISKcomlpex-degr	0.0000216	1/second	(Tigges et al, 2010)
k_miRNAbindRISK	0.00001	1/(molecule*second)	(Tigges et al, 2010)
k-mRNArtTA-to-rtTA	0.00033333	1/second	(Tigges et al, 2009;Tigges et al, 2010)
k-mRNrtTA-degr	0.000288	1/second	(Tigges et al, 2009)
k-Cells-to-mRNArtTA	0.0467	1/second	(Tigges et al, 2009)
k-mRNAamCyan-degr	0.000288	1/second	(Tigges et al, 2009)
kOFF-rtTA-DoX-geneA-binding	0.00001	1/second	(Tigges et al, 2009)
kON-rtTA-DoX-geneA-binding	0.000000028	1/(molecule*second)	(Tigges et al, 2009)
kON-rtTA-DoX-binding	0.00001	1/(molecule*second)	(To & Maheshri, 2010)
kOFF-rtTA-DoX-binding	0.00000002	1/second	(To & Maheshri, 2010)
kON-rtTA-DoX-geneB-binding	0.000000028	1/(molecule*second)	(Tigges et al, 2009)
kOFF-rtTA-DoX-geneB-binding	0.00001	1/second	(Tigges et al, 2009)

k-rtTA-degr	0.000096667	1/second	(Tigges et al, 2009)
k-DoX-rtTA-degr	0.000096667	1/second	(Tigges et al, 2009)
k-geneB-to-mRNAamCyan	0.0467	1/second	(Tigges et al, 2009)
k-mRNAamCyan-to-amCyan	0.00033333	1/second	(Tigges et al, 2009;Tigges et al, 2010)
k-amCyan-degr	0.000096667	1/second	(Tigges et al, 2009)

1.2. "Noisy" simulations

In order to account for the copy-number (*i.e.*, extrinsic) variability we measured experimentally the output distribution (Supplementary Figure 1C) of a transiently-transfected plasmid encoding a ZsGreen1 fluorescent protein. The amplitude of the measured fluorescence was arbitrarily assigned to correspond to 100 plasmid copies and the distribution was rescaled in copy-number units assuming linear relationship between the fluorescence and the copy-number. Plasmid copy-number was then picked randomly from that distribution (Supplementary Figure 1D) and used as an initial condition for each code execution. Furthermore, we used control experiments to estimate intrinsic variability in our circuits. The scontrol constructs (Supplementary Figures 1E, 3F) were transfected using 500 ng of the plasmid in the presence of 1000 ng/mL Dox and the fluorescence measured after 48h. The data was processed as usual (Supplementary Figures 2A-D) to generate the coefficient of variations for the individual bins. The CV of the bidirectional promoter was found to be is ~ 0.25 and the IRES junction ~ 0.30 (Supplementary Figure 1H). Next, we produced normal distributions (Supplementary Figures 1I, 1J) with zero mean and

standard deviation equaling 25% of 0.0467 sec^{-1} (the parameter values representing transcription rate from the bidirectional promoter used in simulations), and zero mean and standard deviation equaling 30% of 0.00033 sec^{-1} (the parameter values representing baseline translation rate). These distributions served to provide absolute perturbations of the original parameter values. Specifically, for each single-cell simulation, the baseline kinetic parameters are perturbed from their original values (k_{TRE}=0.0467 sec^{-1} and k_{IRES}=0.00033 sec^{-1}) by adding noise: $\mathbf{k_{TRE}=0.0467+\xi_1}$ and $\mathbf{k_{IRES}=0.00033+\xi_2}$. The "noisy" parameters ξ_1 and ξ_2 are selected randomly from the normal distributions described previously.

2. Data normalization

The data illustrated in Figures 3, 4, and 5 are normalized prior to processing in order to facilitate comparison between different circuits. (Note that the data in the supplemental material are not normalized.) As shown in Supplementary Figure 3G we use the flow cytometry scatter plots obtained with the negative control circuit of the transcriptional I1-FFL as the baseline to which we normalize the negative control data of the other motifs by making sure that the 99th percentiles of both the input and output values in the negative control measurements overlap. The normalization coefficients are shown in the table below. The resulting normalized negative controls are shown in Supplementary Figure 3H.

Motif	Multiplier X	Multiplier Y
tI1-FFL	1	1
ptI1-FFL_I	2.535275	2.846414
ptI1-FFL_{II}	1.361198	5.301537
tAM	0.653887	1.911177

3. Fitting of input-output response curves

The fitting was performed with the "Ezyfit" toolbox for Matlab, which enables curve fitting of one-dimensional data using arbitrary (non-linear) fitting functions. The results of Ezyfit, were verified using the nlitfit function in MATLAB prompt (nlinfit estimates the coefficient of a nonlinear regression using least squares estimation).

4. Fitting of input-output response curves

The coefficient of variation were fitted when necessary for illustration using the polyfit function in MATLAB, which finds the coefficients of a polynomial p(x) of degree 3 that fits the data.

5. ODE-based analytical treatment

1 Transcriptional incoherent feedforward motif model

The set of ordinary differential equations that correspond to the Type I incoherent feedforward implementation of Fig. 1a, is as follows.

$$
\begin{aligned}
\frac{dmRNAred}{dt} &= c_1 A^* - c_2 mRNAred \\
\frac{dred}{dt} &= c_3 mRNAred - c_4 red \\
\frac{dmRNALacI}{dt} &= c_8 B^* - c_5 mRNALacI \\
\frac{dLacI_gA}{dt} &= -c_6 LacI_gA + c_7 gA \cdot Lac4 \\
\frac{dgA}{dt} &= c_6 LacI_gA - c_7 gA \cdot Lac4 - c_{10} DT \cdot gA + c_{11} A^* \\
\frac{dgreen}{dt} &= c_{12} mRNALacI - c_{13} green \\
\frac{dDT}{dt} &= c_{16} D \cdot tTA - c_{17} DT - c_{18} DT \cdot gB + c_{19} B^* - c_{10} DT \cdot gA + c_{11} A^* \\
\frac{dtTA}{dt} &= -c_{14} tTA + +c_{15} mRNAtta - c_{16} D \cdot tTA + c_{17} DT \\
\frac{dB^*}{dt} &= c_{18} DT \cdot gB - c_{19} B^* \\
\frac{dmRNAtta}{dt} &= stable - c_{20} mRNAtta \\
\frac{dgB}{dt} &= c_{19} B^* - c_{18} DT \cdot gB \\
\frac{dD}{dt} &= -c_{16} D \cdot tTA + c_{17} DT \\
\frac{dA^*}{dt} &= c_{10} DT \cdot gA - c_{11} A^* \\
\frac{dLacI}{dt} &= -\delta_L \cdot LacI + c_9 mRNALacI - 2 \cdot k_d \cdot (LacI)^2 + 2 \cdot k_u \cdot Lac2 \\
\frac{dLac4}{dt} &= c_6 LacI_gA - c_7 gA \cdot Lac4 - \delta_{L4} \cdot Lac4 + k_{d2} \cdot (Lac2)^2 - k_{d4} \cdot Lac4 \\
\frac{dLac2}{dt} &= k_d \cdot (LacI)^2 - k_u \cdot Lac2 - 2 \cdot k_{d2} \cdot (Lac2)^2 + 2 \cdot k_{d4} \cdot Lac4 - \delta_{L2} \cdot Lac2
\end{aligned}
$$

The variables and constants in the system are as follows:

$stable$ = TETcells

δ_L = degradation rate of LacI monomer

δ_{L2} = degradation rate of LacI dimmer

δ_{L4} = degradation rate of LacI tetramer

k_d = dimmerization rate of LacI

k_u = dissociation rate of LacI dimmer

k_{d2} = dimmerization rate of LacI dimmer

k_{d4} = dissociation rate of LacI tetramer

$mRNAred$ = mRNAdsRed

red = dsRed

$mRNALacI$ = mRNALacI_IRES_mRNAzsGreen1

$LacI_gA$ = LacI_geneA

gA = geneA

$green$ = zsGreen1

$mRNAtta$ = mRNArTTA

DT = DoX_tTA

tTA = tTA

B^* = tTA_DoX_geneB (active gene B)

gB = geneB

D = DoX

A^* = tTA_DoX_geneA (active gene A)

$LacI$ = LacI

$Lac4$ = LacItetramer

$Lac2$ = LacIdimer

c_i's are assorted association and dissociation and degradation/dilution rates

2 Steady states

We now solve for steady states of this system, by setting the right-hand side of the ODE to zero. For notational simplicity, we will write "$a \propto b$" to mean that there is some positive constant k (which depends only on the parameters defining the system) such that $a = kb$.

From the equations for $mRNAred$ and red we have that

$$red \propto A^*$$

and from the equation for $mRNALacI$ that

$$mRNALacI \propto B^*$$

and from the equation for $green$ that $green \propto mRNALacI$ and therefore

$$green \propto B^*$$

as well.

From the equation for free Dox, D, we have that $-c_{16}D \cdot tTA + c_{17}DT = 0$, and when this is substituted into the equation for tTA we obtain that $-c_{14}tTA + c_{15}mRNAtta = 0$, and hence, together with $mRNAtta \propto stable$, which follows from the equation for $mRNAtta$, it follows that

$$tTA = \gamma$$

where γ is some positive constant proportional to $stable$.

Hence, $-c_{16}D \cdot tTA + c_{17}DT = 0$ reduces to $-c_{16}D \cdot \gamma + c_{17}DT = 0$, from which we conclude that

$$DT \propto D\,.$$

The equations for B^* or gB give that $B^* \propto DT \cdot gB$, and the equation for A^* gives that $A^* \propto DT \cdot gA$, which since $DT \propto D$, can be also written as

$$B^* \propto D \cdot gB$$

and

$$A^* \propto D \cdot gA$$

respectively.

Also, substituting $c_{10}DT \cdot gA - c_{11}A^* = 0$ allows simplifying the equation for gA to: $c_6 LacI_gA - c_7 gA \cdot Lac4 = 0$, which gives

$$LacI_gA \propto gA \cdot Lac4$$

and also allows simplifying the equation obtained from the rate of $Lac4$ to

$$\delta_{L4} \cdot Lac4 + k_{d2} \cdot (Lac2)^2 - k_{d4} \cdot Lac4 = 0$$

(note that the equations for DT, $LacI_gA$, and gA provide no additional information; they are automatically satisfied because of stoichiometry).

Letting

$$x = red \quad \text{and} \quad y = green$$

we can summarize the constraints as follows:

$$\begin{aligned} y &\propto D \cdot gA \\ x &\propto D \cdot gB \\ mRNALacI &\propto D \cdot gB \propto x \\ LacI_gA &\propto gA \cdot Lac4 \end{aligned}$$

together with:

$$\begin{aligned} -\delta_L \cdot LacI + c_9 x - 2 \cdot k_d \cdot (LacI)^2 + 2 \cdot k_u \cdot Lac2 &= 0 \\ k_d \cdot (LacI)^2 - k_u \cdot Lac2 - 2 \cdot k_{d2} \cdot (Lac2)^2 + 2 \cdot k_{d4} \cdot Lac4 - \delta_{L2} \cdot Lac2 &= 0 \\ -\delta_{L4} \cdot Lac4 + k_{d2} \cdot (Lac2)^2 - k_{d4} \cdot Lac4 &= 0 \end{aligned}$$

where c_9 has been redefined to account for the proportionality $mRNALacI \propto x$. The last of these equations can be solved for $Lac4$ as a constant multiple of $(Lac2)^2$. The middle equation, once this is substituted, becomes a quadratic equation of the type

$$-Ku^2 - bu + cv^2 = 0$$

relating $v = LacI$ and $u = Lac2$, where b and c are positive constants and

$$K = 1 - \frac{k_{d4}}{\delta_{L4} + k_{d4}} > 0\,.$$

Since $f(u) = -Ku^2 - bu + cv^2$ is an inverted parabola with $f(0) = cv^2 > 0$, there is a unique positive solution

$$\theta(v) = \frac{-b + \sqrt{b^2 + 4cv^2}}{2K}$$

for each v, and this solution is an increasing function of v. So $Lac2 = \theta(LacI)$ may be substituted into the first equation:

$$-\delta_L v + c_9 x - 2k_d v^2 + 2k_u \theta(v) = 0 \tag{1}$$

to give a relation between x and $v = LacI$.

Two special cases are especially interesting.

Case I: Irreversible dimmerizations, low degradation

Suppose that dimmerizations are irreversible, in the sense that $k_{d4} \approx 0$ and $k_u \approx 0$ and that degradations of non-tetramer forms are very slow: $\delta_{L2} \approx 0$ and $\delta_L \approx 0$. In this case, $K = 1$ and $b = 0$, and $\theta(v) = \sqrt{c}v$, and Equation (1) says that $x \propto (Lac2)^2$. Since $Lac4$ is a constant multiple of $(Lac2)^2$, we conclude that

$$Lac4 \propto x\,. \tag{2}$$

Case II: Biphasic behavior

A qualitatively very different situation arises if the following conditions hold: $\delta_{L2} \approx 0$ and $\delta_{L4} \approx 0$ Then, the equations for the LacI forms reduce to:

$$\begin{aligned} -\delta_L \cdot LacI + c_9 x &= 0 \\ k_d \cdot (LacI)^2 - k_u \cdot Lac2 &= 0 \\ k_{d2} \cdot (Lac2)^2 - k_{d4} \cdot Lac4 &= 0 \end{aligned}$$

which implies that

$$Lac4 \propto x^4\,. \tag{3}$$

To finalize the study of steady states, we must use the fact that steady states are not be unique, as there are conserved quantities. The total amounts of gene A and gene B, in bound and unbound form, each should equal the plasmid copy number "u":

$$\begin{aligned} gA + A^* + LacI_gA &= u \\ gB + B^* &= u \end{aligned}$$

Since also $B^* \propto D \cdot gB \propto x$ and $A^* \propto D \cdot gA \propto y$, we write $gA = \beta \frac{y}{D}$, $gB = \alpha \frac{x}{D}$ for some positive constants α and β, we can also write these gene conservation equations as follows:

$$\begin{aligned} \beta \frac{y}{D} + \gamma y + \rho \frac{y}{D} \cdot Lac4 &= u \\ \left(\frac{\alpha}{D} + \mu\right) x &= u \end{aligned}$$

for some ρ, from which we have

$$\beta \frac{y}{D} + \gamma y + \rho \frac{y}{D} \cdot Lac4 = \left(\frac{\alpha}{D} + \mu\right) x \,. \tag{4}$$

Observe that the strength of repression by LacI on the promoter of gene A is represented by the kinetic constant c_7 in the equation for $LacI_gA$, and hence appears by the constant of proportionality in $LacI_gA \propto gA \cdot Lac4$, which is then absorbed into ρ.

Saturated response

In the special Case I discussed above, which leads to (2), Equation (4 gives (after redefinining ρ by multiplying by a positive constant):

$$\beta \frac{y}{D} + \gamma y + \rho \frac{y}{D} x = \left(\frac{\alpha}{D} + \mu\right) x \tag{5}$$

and, if D can be assumed to be approximately constant, provides the following *Michaelis-Menten* form for y (dsRed) as a function of x (green):

$$y = \frac{Vx}{1 + kx} \tag{6}$$

for appropriate positive constants V and K. *The constant k is directly proportional, to the strength of LacI repression.* Observe that, in the unrepressed case, y is simply proportional to x.

The assumption that D, free Dox, is a constant (meaning, it is independent of copy number) is reasonable provided that initial Dox is in abundance. We analyze the effect of this approximation below.

Noise in fluorescence experimental data, as well as autofluorescence, may be modeled by additive noise in both x and y measurements. This can be accounted for by modifying the above formula to the more general form $y = \frac{Vx+W}{1+kx}$. A different parametrization of this last formula:

$$y = \sigma(x) = c \frac{x + a}{x + b} \tag{7}$$

is slightly more convenient for fitting.

Biphasic response

In the special Case II discussed above, which leads to (3), Equation (4 gives (after redefinining ρ by multiplying by a positive constant):

$$\beta\frac{y}{D}+\gamma y+\rho\frac{y}{D}x^4=\left(\frac{\alpha}{D}+\mu\right)x \tag{8}$$

and, if D can be assumed to be approximately constant, provides the following form for y (dsRed) as a function of x (green):

$$y=\frac{Vx}{1+kx^4} \tag{9}$$

for appropriate positive constants V and K. Note that this function increses from zero to some maximal value and then decreases to zero. In that sense, it is "biphasic". Once again, the assumption that D is constant is reasonable provided that initial Dox is in abundance. In any event, we show below the biphasic behavior by simulations on the full model, not assuming that D is constant.

Analysis of assumption that D is constant

The amount of free Dox "D" is in fact dependent on plasmid copy number. To study how this affects results, we use a second conservation law as well, the one that ties Dox in all its forms, bound and unbound:

$$DT+A^*+B^*+D=d_0$$

where d_0 is total initial Dox. Since $x\propto B^*$, $y\propto A^*$, and $DT\propto D$, we can rewrite this as $D+ax+by=d_0$ for some constants a and b (redefining d_0 by constant multiple).

In the case of a saturated response (the biphasic case is similar), this means that we must consider these two equations:

$$\begin{aligned}\beta\frac{y}{D}+\gamma y+\rho\frac{y}{D}x &= \left(\frac{\alpha}{D}+\mu\right)x\\ D+ax+by &= d_0\end{aligned}$$

and eliminate D in order to obtain y as a function of x that is obtained by solving a quadratic equation for y. This can be done with a symbolic computation package. To illustrate, let us pick all constants equal to 1. The solution of

$$\begin{aligned}\frac{y}{D}+y+\frac{y}{D}x &= \left(\frac{1}{D}+1\right)x\\ D+x+y &= 1\end{aligned}$$

that satisfies that $x\leq 1$ ($D+x+y\leq 1$ must be satisfied by all values) is

$$f(x)=1+\frac{1}{2}x-\frac{1}{2}\sqrt{4-4x+5x^2}\,.$$

This function increases for $x<4/5$ and decreases for $x>4/5$. On the interval $[4/5,1]$ the function is always >0.38. This means that $x+f(x)>1$ for $x>4/5$. Thus, on the domain where $D+x+y\leq 1$, the function is increasing and has a "saturating" character, as in the high-D approximation.

3 A simulation

We illustrate biphasic behavior by simulation of the full system (without making the "high D" approximation). Merely for mathematical illustration, all constants are taken equal to one, except for $\delta_{L2} = 0$ and $\delta_{L4} = 0$. Ignoring units, we take the initial amount of D to be $d_0 = 10$, and of gA and gB as u, where u is thought of as a parameter that is proportional to plasmid concentration. The constant *stable* is set to 1. All other initial conditions are set to zero. Figure S6A shows results of simulation runs that used values of u from 0.1 to 20 in steps of 0.1. The biphasic behavior is also observed for the concentrations of *red* and *green* as a function of time, as shown in Figure S6B for the case $u = 20$.

4 Post-transcriptional type 1 incoherent feedforward motif model

We next analyze mathematically a simplified model of the post-transcriptional type 1 incoherent feedforward motif. For simplicity of exposition, we omit a few of the intermediate steps from the full computational model, but a more detailed analysis, analogously to what was that done for the transcriptional incoherent feedforward motif model, could be carried out as well.

We use these species (upper case for species, lower case for concentrations):

M = mRNA (protein is in steady state proportional to M, so is omitted from the model); we also denote the concentration of M as "y" to indicate its role as output variable.

A = gene; this is the input, and will also be called "x".

B = miRNA.

P = RISC.

B^* = activated miRNA (complex BP).

Q = complex of activated miRNA and RISC (QB^*).

The simplified reactions are as follows:

$$A \xrightarrow{c_1} M + B$$

$$B + P \underset{c_3}{\overset{c_2}{\rightleftarrows}} B^*$$

$$B^* + M \xrightarrow{c_4} Q$$

$$M \xrightarrow{c_5} 0$$

$$B \xrightarrow{c_6} 0$$

$$Q \xrightarrow{c_7} B^*$$

which lead to the following differential equations:

$$\begin{aligned}
\frac{dm}{dt} &= c_1 a - c_4 b^* m - c_5 m \\
\frac{db}{dt} &= c_1 a - c_2 bp + c_3 b^* - c_6 b \\
\frac{db^*}{dt} &= c_2 bp - c_3 b^* - c_4 b^* m + c_7 q \\
\frac{dq}{dt} &= c_4 b^* m - c_7 q \\
\frac{dp}{dt} &= -c_2 bp + c_3 b^*
\end{aligned}$$

together with the conservation law for total RISC:

$$p + b^* + q \equiv c$$

where c is some positive constant. At steady state, from $\frac{dm}{dt} = 0$ we obtain:

$$m = \frac{c_1 a}{c_5 + c_4 b^*}, \tag{10}$$

from $\frac{p(b+b^*+q)}{dt} = 0$ we obtain:

$$b = \frac{c_1}{c_6} a, \tag{11}$$

from $\frac{db}{dt} = 0$ and using (11):

$$b^* = \frac{c_2}{c_3} bp = \frac{c_1 c_2}{c_3 c_6} ap, \tag{12}$$

and finally from $\frac{dq}{dt} = 0$:

$$q = \frac{c_4}{c_7} b^* m = \frac{c_1 c_2 c_4}{c_3 c_6 c_7} apm, \tag{13}$$

so, substituting (12)-(13) in the conservation law, we have also:

$$p \left[1 + \left(\frac{c_1 c_2}{c_3 c_6} + \frac{c_1 c_2 c_4}{c_3 c_6 c_7} m \right) a \right] = c. \tag{14}$$

Substituting (12) in (10), we conclude that:

$$y = \frac{Vx}{K + px} \tag{15}$$

and that p is related to x and y via (14), which we write as:

$$p\,[1 + [r + sy]x] = C, \tag{16}$$

where we have defined:

$$V = \frac{c_3}{c_4},\ K = \frac{c_3 c_5}{c_1 c_4},\ r = \frac{c_1 c_2}{c_3 c_6 c_7},\ s = r\frac{c_4}{c_7}.$$

Note that, given any V, K, r, s, one can always find c_i's such that these formulas hold (pick c_1, c_4, c_6 arbitrary and then $c_3 = Vc_4$, $c_2 = \frac{rVc_4c_6}{c_1}$, $c_5 = \frac{Kc_1}{V}$, $c_7 = \frac{r}{s}c_4$), so that the general case is captured by these new constants.

We next perform an approximate analysis, assuming that $C \gg 1$ (total RISC is very large).

For small values of x, we have that y should also be small, and thus (16) is approximated by $p = C$, which means that (15) is approximately:

$$y = \frac{Vx}{K + Cx},$$

which is a saturation function.

On the other hand, consider the behavior when x is large. Using that for large x, px is approximately $\frac{C}{r+sy}$, it follows that px is bounded, and it goes to zero provided that $y \to \infty$. So, in (15), we have that y becomes approximately equal to the linear function $\frac{V}{K}x$ provided that $y \to \infty$ (because $px \to 0$), and is in any case of linear growth.

Actually, it is always the case that $y \to \infty$. Indeed, from:

$$p\,[1 + [r + sy]x] \;=\; C$$

we have that:

$$p\,x \;=\; \frac{C}{1/x + (r + sy)} \;<\; C/r\,,$$

and therefore:

$$y \;=\; \frac{Vx}{K + px} \;>\; k\,x\,,$$

where

$$k \;=\; \frac{V}{K + C/r}\,,$$

which proves that $y \to \infty$, as claimed.

We verify these conclusions (without the approximation) with a plot of $y = y(x)$ obtained by numerically solving for p in (16), substituting in (15), and taking the positive root of the resulting quadratic equation. We pick for simplicity all constants $c_i = 1$, and total RISC $c = 1000$. We expect a behavior $y = \frac{x}{1+1000x}$, which saturates at $y = 0.001$ for small x, and asymptotically a linear behavior asymptotically with slope 1 for large x. The latter is clearly seen in Figure S6C. To appreciate the former, we zoom into the initial part of the above plot in Figure S6D.

To help visualize the two regimes, Figure S6E provides a a plot of the derivative dy/dx. Note the initial slope near zero (adaptation behavior) and final slope near 1 (linear behavior) .

6. DNA sequences of structural features

LacO sequence variants

Type	Sequence
Wild type	CGGTCTAGGTTGTGGAATTGTGAGCGCTCACAATTCTAGGTTGTGGAATTGTGAGCGCTCACAATTA
1st mutant	CCGGTCTAGGTTGTGAATTGTGAGCGGATAACAATTCTAGGTTGTGAATTGTGAGCGGATAACAATTA
2nd mutant	CCGGTCTAGGTTGTGAATTGTGACCGGATAACAATTCTAGGTTGTGAATTGTGACCGGATAACAATTA
3rd mutant	CCGGTCTAGGTTGTGAATTGTGAGGGGATAACAATTCTAGGTTGTGAATTGTGAGGGGATAACAATTA
4th mutant	CCGGTCTAGGTTGTGAATTGTAAGCGGATAACAATTCTAGGTTGTGAATTGTAAGCGGATAACAATTA
Negative Control	CCGGTCTAGGTTGTGTAGACTGAGACGTGGAGATCTCTAGGTTGTGTAGACTGAGACGTGGAGATCTA

RNAi target sequence

Type	Sequence
FF3	TTTGTATTCAGCCCATATCGTT

7. Summary of experimental conditions

DNA constructs used to implement the motifs

tI1-FFL-Wild Type	pTRE-Tight-BI-LacI-IRES-ZsGreen1-LacO-DsRed
tI1-FFL-Mutant 1	pTRE-Tight-BI-LacI-IRES-ZsGreen1-$LacO_{1st\ mt}$-DsRed
tI1-FFL-Mutant 2	pTRE-Tight-BI-LacI-IRES-ZsGreen1-$LacO_{2nd\ mt}$ -DsRed
tI1-FFL-Mutant 3	pTRE-Tight-BI-LacI-IRES-ZsGreen1-$LacO_{3rd\ mt}$ -DsRed
tI1-FFL-Mutant 4	pTRE-Tight-BI-LacI-IRES-ZsGreen1-$LacO_{4th\ mt}$ -DsRed
tI1-FFL-NegCon	pTRE-Tight-BI-LacI-IRES-ZsGreen1-$LacO_{NegCtrl}$ -DsRed
ptI1- FFL_I Wild Type	pTRE-Tight-BI-DsRed-miR-F3-AmCyan-F3

ptI1- FFL_{II} Wild Type	pTRE-Tight-BI-DsRed-miR-FF3/tgt-FF3-AmCyan
ptI1-$FFL_{I/II}$ NegCon	pTRE-Tight-BI-DsRed-miR-FF3-AmCyan-FF4x3
tAM-1xLacO	pTRE-Tight-BI-1xLacO-LacI-IRES-ZsGreen1-DsRed
tAM-2xLacO	pTRE-Tight-BI-2xLacO-LacI-IRES-ZsGreen1-DsRed
tAM-NegCtrl	pTRE-Tight-BI-2xLacO-LacI-IRES-ZsGreen1-DsRed with 1 M IPTG

Experiments shown in Figure 3

Motif	Reagent	Wait time	Plasmid Amount	Dox
tI1-FFL-Wild Type	LipoLTX	48h	500 ng	1000 ng/ml
tI1-FFL-Mutant 1	LipoLTX	48h	500 ng	1000 ng/ml
tI1-FFL-Mutant 2	LipoLTX	48h	500 ng	1000 ng/ml
tI1-FFL-Mutant 3	LipoLTX	48h	500 ng	1000 ng/ml
tI1-FFL-Mutant 4	LipoLTX	48h	500 ng	1000 ng/ml
tI1-FFL-NegCon	LipoLTX	48h	500 ng	1000 ng/ml

Experiments shown in Figure 4

Motif	Reagent	Wait time	Plasmid Amount	Dox
ptI1- FFL_{I} Wild Type	LipoLTX	48 h	500 ng	1000 ng/ml
ptI1- FFL_{II} Wild Type	LipoLTX	48 h	500 ng	1000 ng/ml

ptI1- $FFL_{I/II}$ NegCon	LipoLTX	48 h	500 ng	1000 ng/ml

Experiments shown in Figure 5

Motif	Reagent	Wait time	Plasmid Amount	Dox
tAM-1xLacO	LipoLTX	48 h	500 ng	1000 ng/ml
tAM-2xLacO	LipoLTX	48 h	500 ng	1000 ng/ml
tAM-NegCtrl	LipoLTX	48 h	500 ng	1000 ng/ml

Primers used for cloning purposes

Primer P1	CCAACGCGTCCACCATGGCCCTGTC
Primer P2	CCAGCTAGCTTATCCGGAGAAGGGCACCA
Primer P3	ACATATTTGAATGTATTTAGAAAAAT
Primer P4	AGTGAGCGAGGAAGCTCGGGGCAG
Primer P5	GTTGTCCATGGTGGCGAGACCGGTTGG
Primer P6	CCATCTAGATTACTACTGGGAGCCGGAGTG
Primer P7	CTGCAGCTTGGCGGTCTGG
Primer P8	CCAGCTAGCTTACGCTTACAATTTACGCGTTAAGATAC
Primer P9	CCAGCCGGGCCTCCCACCATGAAACCAG
Primer P10	CGAATTCTGCAGTCGACGGTAC
Primer P11	CCAGGATCCTCAGGGCAAGGCGGA
Primer P12	CTGGAGATATCGTCGACAAGC
Primer P13	AGTGAGCGAGGAAGCTCGGGGCAG
Primer P14	ACATATTTGAATGTATTTAGAAAAAT
Primer P15	CCTCGCCCTCGATCTCGAAGTA
Primer P16	CCGTCAGATCGCCTGGAGAA
Primer P17	CCTCGCCCTCGATCTCGAAGTA

Primer P18	CCAGCTAGCCCTCCCACCATGAAACCAG
Primer P19	CCAGAATTCTTACGCTTACAATTTACGCGTTAAGATAC
Primer P20	CATGACCTTATGGGACTTTCCTAC
Primer P21	TACGCGTTAAGATACATTGATGAG
Primer P22	CGTCAATGGGAGTTTGTTTTG
Primer P23	GCTGGCATAAATATCTCACTCG
Primer P24	CCAGCTAGCCTCGCCACCATGGACAAC
Primer P25	CACCCGGGCTACTGGGAGCCGGAGTG
Primer P26	GGGACTTTCCAAAATGTCGTAAC
Primer P27	CCACCCGGGCGAGCTCGAAATCTCCAGGC
Primer P28	CCAGATATCCGAGACCGGTCTAGGTTGTG
Primer P29	CCTCGCCCTCGATCTCGAAGTA
Primer P30	CCAGATATCCGAGACCGGTCTAGGTTGTG
Primer P31	GCCTTTCTTGTTCCGGTGTTAAAAACGCCACCATGGCCCTGTC
Primer P32	TTGTCTCTTGCTGGTGTTCGAAAAACGCTTACAATTTACGCGTTAAGATAC
Primer P33	AACACCGGAACAAGAAAGGCTTTTGCAGGTGGCCCCCGCGGCATATGAC
Primer P34	CGAACACCAGCAAGAGACAATTTTGCAGGTGGACGTCAGGTGGCACTTTTCG
Primer P35	CCACGGCCGGAAGCTTGTTAAGCTCGAGATCTGA
Primer P36	CCACGGCCGAGGATCCACCGGATCTAGATAACTG
Primer P37	CACTTACATATGTCAGATCCGCTAGCGCTAC
Primer P38	CTACAACATATGTTATCGAGATCTGAGTCCGGAGAA
Primer P39	CAACTGCTTCGAGCACAAGT
Primer P40	ACATTTCCCCGAAAAGTGC
Primer P41	ATCAGCCTGAAGGGCAACTG
Primer P42	CTGAGTCCGGAGAAGGGCAC
Primer P43	GCCACCACCTGTTCCTGAGATC
Primer P44	TTATCTAGATCCGGTGGATCCC
Primer P45	GCGTGATGAACTTCGAGGAC

Oligos used for cloning purposes

Oligo O1	CCGGTCTAGGTTGTGGAATTGTGAGCGCTCACAATTCTAGGTTGTGGAATTGTGAGCGCTCACAATTA
Oligo O2	CCGGTAATTGTGAGCGCTCACAATTCCACAACCTAGAATTGTGAGCGCTCACAATTCCACAACCTAGA
Oligo O3	GGCCGCCGCTTGAAGTCTTTAATTAAACCGCTTGAAGTCTTTAATTAAACCGCTTGAAGTCTTTAATTAAAC
Oligo O4	GGCCGTTTAATTAAAGACTTCAAGCGGTTTAATTAAAGACTTCAAGCGGTTTAATTAAAGACTTCAAGCGGC
Oligo O5	AGCTTACTAACATGCTTCGAAACGATATGGGCTGAATACAAAG
Oligo O6	TCGACTTTGTATTCAGCCCATATCGTTTCGAAGCATGTTAGTA

siRNAs used targeting AmCyan

siRNA-1	GCCACUACUUCACCGUGAAUU **GCCGGUGAUGAAGUGGCACUU**
siRNA-7	CCUCCUACAAGACCAAGAAUU **GUGGAGGAUGUUCUGGUUCUU**

8. DNA Plasmids

pTRE-Tight-BI-AmCyan-DsRed: AmCyan gene was amplified from the AmCyan-C1 plasmid (Clontech) using primers P1 and P2 with NheI and MluI restriction sites. The product was digested with NheI and MluI and repurified. In parallel, pTRE-Tight-BI (Clontech) was digested with NheI and MluI and gel-purified. The digested insert was ligated into the digested vector at 1:2 ratio at 12 ^{o}C overnight, transformed and expanded. The construct was sequenced using primers P3 and P4. The DsRed-monomer gene was amplified from the pCAGOP-DsRed-Monomer-N1 plasmid (Rinaudo et al, 2007) using primers P5 and P6 with XbaI and AgeI restriction sites. The PCR product was digested with XbaI and AgeI enzymes. In parallel, the above pTRE-Tight-BI-AmCyan plasmid was digested with XbaI and AgeI and gel-purified. The digested DsRed-monomer insert was ligated into the digested vector at 1:1 ratio at 14 ^{o}C overnight, transformed and expanded. Correct constructs were identified by double EagII and BglII digestion and by observing fluorescence in transfected cells.

pTRE-Tight-BI-AmCyan-LacO-DsRed: pTRE-Tight-BI-AmCyan-DsRed was digested by AgeI and purified. The backbone was dephosphorylated and purified. Oligos O1 and O2 (Sigma) containing a tandem repeat of the wild type LacO sequence CTAGGTTGTGGAATTGTGAGCGCTCACAATT were gel-purified using 20% denaturing PAGE and annealed. The double-stranded LacO insert with AgeI-compatible sticky ends was phosphorylated and ligated into AgeI-digested and purified pTRE-Tight-BI-AmCyan-DsRed backbone at 1:3 ratio at 14 ^{o}C overnight. The ligation product was transformed and expanded. LacO sites integrity was verified by sequencing with P7.

pTRE-Tight-BI-LacI-LacO-DsRed: LacI gene was amplified from CMV-LacI-F3x3 (Rinaudo et al., 2007) using primers P8 and P9 with XmaI and NheI restriction sites and digested with these enzymes. In parallel, pTRE-Tight-BI-AmCyan-LacO-DsRed was digested with XmaI and NheI to remove AmCyan sequence. The digested LacI insert was ligated into the gel-purified backbone vector at 1:4 ratio at 14 ^{o}C overnight, transformed and expanded. The correct clones were verified by separate NheI and BglII digestions.

pTRE-Tight-BI-LacI-IRES-ZsGreen1-LacO-DsRed: IRES-ZsGreen1 sequence was amplified from pIRES2-ZsGreen1 (Clontech) using primers P10 and P11 with BamHI restriction sites, and digested with BamHI. In parallel, pTRE-Tight-BI-LacI-LacO-DsRed was digested with BamHI, gel-purified and dephosphorylated. The digested IRES-ZsGreen1 insert was ligated into the digested vector at 1:4 ratio at 14 ^{o}C overnight, transformed and expanded. The clones were verified by sequencing with primers P12, P13, and P14.

pTRE-Tight-BI-LacI-IRES-ZsGreen1-LacO$_X$-DsRed (X = 1st mt, 2nd mt, 3rd mt, 4th mt and NegCtrl): LacO mutant inserts with AgeI-compatible sticky ends were prepared similarly to the

wild-type LacO insert. pTRE-Tight-BI-LacI-IRES-ZsGreen1-LacO-DsRed was digested by AgeI and gel-purified. The backbone and the inserts were ligated at 1:3 ratio at room temperature for 10 minutes, transformed and plated. Colonies were analyzed by colony PCR using primers P15 and P16, positive colonies were expanded overnight, plasmid DNA was isolated and the results were verified by sequencing with primer P17.

LacI-FF3-pIRES2-ZsGreen1: LacI gene with the FF3 siRNA target in the 3'-UTR was amplified from CMV-LacI-FF3 (Rinaudo et al, 2007) using primers P18 and P19 with NheI and EcoRI restriction sites. pIRES2-ZsGreen1 vector and LacI amplicon were digested with NheI and EcoRI enzymes, and vector DNA was gel-purified and dephosphorylated. The digested backbone and insert were ligated at 1:2 ratio overnight, transformed and plated. Colonies were analyzed by colony PCR using primers P20 and P21. Positive colonies were expanded, and the clones were verified by sequencing with primers P22 and P23.

DsRed-pIRES2-ZsGreen1: DsRed-monomer gene was amplified from the pCAGOP-DsRed-Monomer-N1 plasmid (Rinaudo et al, 2007) using primers P24 and P25 with NheI and XmaI restriction sites. LacI-FF3-pIRES2-ZsGreen1 plasmid and the PCR product were digested by NheI and XmaI enzymes and gel-purified. Gel-purified backbone and insert were ligated at a 1:3 ratio at room temperature for 10 minutes, transformed, plated and expanded. Clones were verified by sequencing with primer P26.

pTRE-Tight-BI-1xLacO-LacI-IRES-ZsGreen1-DsRed and **pTRE-Tight-BI-2xLacO-LacI-IRES-ZsGreen1-DsRed**: These plasmids were constructed from pTRE-Tight-BI-LacI-IRES-ZsGreen1-LacO-DsRed by inverting the region between the LacI and the DsRed genes that contains the bidirectional promoter and the LacO sequences. The backbone vector excluding this

region was amplified using primers P27 and P28 with XmaI and EcoRV restriction sites, respectively. The PCR product was gel-purified, digested using XmaI and gel-purified once more. The backbone vector was digested with SacI (which removed the pTRE-LacO region) and purified. Digested vector was blunted with Mung Bean Nuclease, digested with AgeI and gel purified. The insert and backbone, with one side having compatible AgeI and XmaI sticky ends and the other side blunt ends, were ligated at 1:1 and 1:2 ratios at 16 ^{o}C overnight and transformed into EPI300 E. Coli (Epicentre). Plasmid DNA was sequenced with primer P29. Two separate colonies resulting from the 1:1 and 1:2 ligations respectively yielded constructs with single and double repeats of the LacO.

pTRE-Tight-BI-DsRed-miR-FF3-AmCyan-FF3: pCMV-AmCyan-FF3 was constructed by replacing ZsYellow1 in pCMV-ZsYellow1-FF3 (Rinaudo et al, 2007) with AmCyan from pAmCyan-C1 (Clontech) by using NheI and BglII. AmCyan-FF3 was amplified from pCMV-AmCyan-FF3 with primers P31 and P32, and chewed back with 1.2 U T4 polymerase in the presence of 1mM dTTP at 27 °C for 5 min. DsRed-miR-FF3 was amplified from pTRE-tight-bi-DsRed-FF3(Leisner et al, 2010) with primers P33 and P34 and chewed back with 1.2 U T4 polymerase in the presence of 1 mM dATP at 27 °C for 5 min. Chew-back reactions were stopped by heat-inactivation of T4 polymerase at 75 °C for 20 min. Then two chewed DNA fragments were annealed by gradually lowering the temperature from 75 °C to 25 °C. The product was transformed into EPI300.

pTre-Tight-BI-DsRed-miR-FF3-AmCyan (negative control for pTI1-FFL circuits): The AmCyan coding sequence from pAm-Cyan-C1 was amplified using primers P37 and P38 with NdeI sites. The PCR product and pTRE-tight-bi-DsRed-FF3 (Leisner et al, 2010) were digested with NdeI, backbone DNA was dephosphorylated, and the two were ligated at 1:3 ratio. The

construct was transformed and plated. Colonies were tested by PCR using primers P39 and P40, followed by sequencing using primers P41 and P42.

pTRE-Tight-BI-DsRed-miR-FF3/tgt-FF3-AmCyan: Synthetic FF3 sites with HindIII and SalI-compatible sticky ends were synthesized (IDT) by annealing and phosphorylating O5 and O6. pTre-Tight-BI-DsRed-FF3-AmCyan backbone was digested with HindIII and SalI and subsequently ligated with the synthetic insert. Constructs were transformed and plated. Colonies were tested using primers P43 and P44, expanded and sequenced using primer P45.

9. Cloning kits

PCR product purifications were performed using the Qiagen PCR purification kit. Gel-purifications were performed using Qiagen Gel Purification kit from 1% agarose gel. DNA isolations were performed using Qiagen MiniPrep kit. Sequencing was performed by Genewiz.

Supplemental References

Hsieh M, Brenowitz M (1997) Comparison of the DNA Association Kinetics of the Lac Repressor Tetramer, Its Dimeric Mutant LacI adi , and the Native Dimeric Gal Repressor. *Journal of Biological Chemistry* **272:**22092-22096.

Leisner M, Bleris LG, Lohmueller J, Xie Z, Benenson Y (2010) Rationally designed logic integration of regulatory signals in mammalian cells. *Nature Nanotechnology* **5:** 666-670

Ozbudak EM, Thattai M, Lim HN, Shraiman BI, Van Oudenaarden A (2004) Multistability in the lactose utilization network of Escherichia coli. *Nature* **427:**737-740

Rinaudo K, Bleris LG, Maddamsetti R, Subramanian S, Weiss R, Benenson Y (2007) A universal RNAi-based logic evaluator that operates in mammalian cells. *Nature Biotechnology* **25:**795-801

Tigges M, Marquez-Lago T, Stelling J, Fussenegger M (2009) A tunable synthetic mammalian oscillator. *Nature* **457:**309

Tigges M, Dénervaud N, Greber D, Stelling J, Fussenegger M (2010) A synthetic low-frequency mammalian oscillator. *Nucleic Acids Research* **38:**2702-2711

To T, Maheshri N (2010) Noise Can Induce Bimodality in Positive Transcriptional Feedback Loops Without Bistability. *Science* **327:**1142-1145